

# **MICROSEISMIC IMAGING OF A GEOTHERMAL RESERVOIR STIMULATION**

**B.C. Dyer, U. Schanz, T. Spillmann, F. Ladner and M.O. Häring**

## **Introduction**

Exploitation of the geothermal heat energy from rocks at several kilometres depths has been the goal of various projects since the mid 1970's. Initially this type of resource was referred to as Hot Dry Rock (HDR) but is now generally known as an Enhanced/Engineered Geothermal System (EGS). Tester et. al., 2006 provide a comprehensive review of the projects, completed and in progress, and of the technologies involved. To exploit the energy contained in these deep rocks poses technical challenges in drilling, well completion, creation of the heat exchange reservoir at depth and control of seismicity. In spite of the difficulties, EGS offers the potential prize of almost limitless clean energy, so it is not surprising that this technology continues to attract investors prepared to take a higher risk than is involved in developing more established renewable energy resources. However, commercial energy production from the greatest potential resource, hot rock at >5km depth or >200°C, remains elusive.

The basic principle in exploiting the heat energy stored in rocks at depth is to circulate water through the rock to extract the heat. Typically the rocks that are targeted are not porous and the flow paths are through natural fractures. One of the problems in developing EGS resources is that there is no surface based means of exploring for fractures that may be steeply dipping, at the required depths. As such, the first well in a new area being investigated for geothermal production may be considered as an exploration well.

To achieve economic flow rates the natural fractures commonly require stimulation to reduce the flow impedance. Stimulation can generate thousands of microseismic events and critically a few small earthquakes that may be felt at the surface. The microseismic and hydraulic data derived from the stimulation enable the potential for developing a fractured reservoir to be evaluated. However, the observed earthquake magnitudes may alone determine if further development is possible if the magnitudes exceed local limits or cause public concern.

The subject of this paper is an EGS project in Basel, Switzerland that aimed to create a cogeneration pilot plant producing both electrical and thermal energy for district heating. As the geothermal project is located within the city the potential of generating earthquakes that might be felt or posed a risk to public safety, was a critical consideration. In view of this the installation and operation of a sensitive and highly reliable seismic monitoring system was a key priority of the project.

In order to accurately locate the microseismic events an accurate velocity model was required. It is described here how using a deep seismic sensor in the stimulation well it was possible to derive the velocity model directly from the microseismic data. Real time monitoring of the microseismic event distribution enabled the growth of the stimulated region to be observed and the reservoir properties to be interpreted and evaluated. It is also shown how potential fractures, that were not stimulated but could be of interest for developing the reservoir, may be imaged by migration of the microseismic data.

### **The geological and tectonic framework**

The Basel project is located in the Upper Rhine Graben (Figure 1) that forms a part of the European Cenozoic rift system. Extension in the Upper Rhine Graben was controlled by pre-existing structures in the basement and accommodated by the formation of normal faults and flexures (Figure 1; Laubscher, 1970; Illies, 1981; Gürler et al., 1987; Lacombe et al., 1993; Ustaszewski et al., 2005). Several NNE-SSW and NW-SE trending fault systems of various ages are observed in the eastern part of the project area (Figure 1).

The azimuth of the maximum horizontal principal stress ( $S_{Hmax}$ ) has been deduced from UBI log analysis in the granite section of Basel 1. The direction of  $S_{Hmax}$  was determined from borehole breakouts as  $N143\pm 14^\circ E$  and from drilling induced tensile fractures as  $N151\pm 13^\circ N$  (Valley and Evans, 2006; Figure 2). The fracture strike directions, also measured from the UBI log, were predominantly in the range  $140^\circ$  to  $170^\circ$  (Figure 2). These measurements are consistent with previous estimates of the direction of  $S_{Hmax}$  of  $150^\circ$  and  $145^\circ$  (Plenefisch und Bonjer, 1997; Evans and Roth, 1997, respectively). The maximum horizontal stress direction is a result of the alpine compression which is the predominant mechanism for the natural seismic activity in the area, and not the extension of the Rhine graben, a failed rift system that predates the forces acting at present.

The depths of the major lithological units were interpreted from the cuttings and well logs after drilling the borehole Basel 1, as follows. The granitic basement was found at  $\sim 2257$  m bOD, overlain by the Carboniferous/Permian from  $\sim 1396$  m bOD and the Mesozoic from  $\sim 147$  m bOD with Tertiary sediments and a thin alluvial layer above. The local ground surface is at 251 m aOD.

### **Monitoring System**

The microseismic monitoring network consisted of six permanent, 3 component downhole geophones. Four of these tools were installed at moderate depths between 325 m and 550 m

below the surface, Otterbach 1, Haltingen, St. Johann and Schützenmatte (Figure 1). The geophone in Riehen 2 was installed at 1178 m and the deepest geophone in Otterbach 2 is in the granite at a depth of 2738 m below the surface. A special 200°C, 100MPa geophone tool was built and temporarily installed in Basel 1 to calibrate the seismic velocity model. The tool was intended to rest on the bottom of the well but stopped at 4422 m bOD where the borehole had become impassable, but not hydraulically blocked, during pre-stimulation hydraulic tests.

In view of the known natural seismicity and the potential seismic risks it was a major concern to have a clear understanding of the natural microseismicity in the target area prior to any hydraulic tests. Installation of the seismic monitoring system commenced 3 months prior to the drilling of the first well, Basel 1 and was fully operational 6 months prior to the first hydraulic injection so that the drilling of the second half of the well in the hot, fractured granite could be fully monitored. Continuous operation of the monitoring system during the drilling and subsequent stimulation of the well was critical in meeting the public approval to monitor and provide an immediate response to significant earthquakes or ground shaking. In order to minimise any potential downtime of the microseismic network there were sufficient spares to replace any of the permanent receivers, downhole cables and data acquisition units at each receiver station. During the main stimulation and pre-stimulation a field team was on standby to replace any borehole receiver within 36 hours. The trace data from the network stations were continuously transferred via a virtual private network (VPN) link to the central server and data acquisition system, which were also duplicated, and the data were continuously backed up to computer disk and optical storage media.

Injection rate and hydraulic pressure were monitored at the wellhead. Hydraulic pressure was also monitored at depth. Unfortunately, after the pre-stimulation test the borehole was impassable at 4422 m bOD such that downhole logging could not be conducted below this depth.

Prior to the stimulation experiments the network resolution was tested by analysing the location errors over a synthetic hypocenter grid with a 50 m grid spacing. P and S traveltimes from each grid point to the receivers were compared with traveltimes from trial locations around the grid point. By limiting the maximum traveltime differences between the grid point and trial location, for each receiver, to the picking accuracy of  $\pm 8$ ms, an error surface around each grid point was obtained. The resolution was defined to be the maximum distance between the grid point and the error surface. The method available at the time was limited to constant  $V_P$  and  $V_S$  velocities to calculate the resolution times rather than the two layer model used for the actual locations and so the error values should be treated as estimates. However, from this analysis of the network resolution it was found that the monitoring stations St. Johann and Otterbach 1 had relatively little influence on the resolution and did not need to

be routinely processed.

The resolution of a network of Haltingen, Schützenmatte, Riehen and Otterbach 2 is shown for a horizontal slice at the reservoir depth and a S-N vertical section in Figure 2. These estimated errors are consistent with the traveltimes misfits of the real locations and the apparent resolution of the locations that can be assessed from the dimensions of the seismically mapped features in the hypocenter distribution. It should be noted that the resolution shown is the relative resolution between events due to the traveltimes picking accuracy. The absolute resolution depends on the accuracy of the velocity model as well.

### **Seismic Response Procedure**

Prior to the commencement of the stimulation a response procedure was devised that specified the actions to be taken for a range of scenarios. This system was based on the “Traffic Light” scheme of Bommer et. al., 2006 and adapted to local conditions. Three independent criteria were considered in the procedure: Responses from the public, local magnitude ( $M_L$ ) and peak ground velocity (PGV). The  $M_L$  and PGV levels were derived from simulations of surface ground motion based on real event data from the Soultz-sous-Forêts EGS project (Baria et. al., 2006) and the geological situation (microzonation) in Basel (Rutishauser, 2006). The seismic levels and corresponding hydraulic responses are shown in Figure 4. It was not possible to quantify the public response in advance. None the less, the interpretation of the public response was the overriding consideration. The full procedure also included a reporting hierarchy from the duty geophysicist to the exploration company, civil authorities and public that followed the same levels.

The local earthquake magnitude ( $M_L$ ) and ground velocity were provided by the Swiss Seismological Service (SED) using an automatic system backed up with visual checks. The SED derived the magnitudes from their own seismometer network and so were completely independent monitors. This approach also ensured consistency with the magnitudes of regional earthquakes. The SED locations and magnitudes were posted to a public web site in near real time. These event parameters were monitored by the duty geophysicist using an internet based earthquake notification system (referred to as a CISN display, [www.cisn.org](http://www.cisn.org)) and were backed up by mobile telephone and Email alerts from the SED.

The permanent microseismic network provided alternate measures of the moment magnitude ( $M_W$ ) that could be loosely related to the SED measure of  $M_L$ . The real time processing software continuously monitored these levels and incorporated internal audible alarms and visual updates on screen to alert the operators to potential events requiring a response. This system was staffed 24 hours a day during the stimulation by at least one geophysicist and an

operator which enabled immediate visual checks to be made and the response procedure to be followed within minutes of an event. The duty geophysicist also filed reports with the SED for all events greater than 2.0M<sub>L</sub> that provided data from the permanent seismic network and plots of the hydraulic data from the start of the stimulation up to the event time.

### **Velocity Model**

An accurate velocity model is essential to obtain accurate absolute event locations. As all the sensors were located in the sediments or the granite, a velocity model with two horizontal layers (sediments and crystalline) was considered to be appropriate. Initially, average P and S velocities in each layer were obtained from sonic velocity measurements. In principle, the average velocities in the sediments and granite could have been refined by firing check shots in the well over the reservoir interval. However, due to the proximity of domestic properties and sources of radio interference it would have been necessary to use radio frequency safe detonators. Suitably safe detonators were available but had a 150°C temperature limit that would have required prior cooling of the well to be met. This was possible but in preference two alternative methods were tested.

In the first, a drilling jar was tested as a source. The jars were fired just below the top of the granite to measure the sediment velocities directly and as a transmission test from an interim depth prior to the planned terminal depth of the well at >5000m. Although 21 jars were fired for stacking purposes, the jars were not sufficiently energetic to be detected at all stations. Only S waves were detected at the two nearby receivers Otterbach 2 and Haltingen.

The second option was a combined determination of hypocenter locations and velocities. To minimise non-uniqueness in the solution, a deep geophone in the reservoir interval was required. The only option was to deploy a tool into the stimulation well, Basel 1. However, the tool could only be deployed at the start of the stimulation as access to the well was required subsequently for production logging.

Over the 40 hour period when the geophone was deployed in Basel 1, the event locations were predominantly within around 100m of the geophone. Two types of response were observed: In the first, just a single arrival was detected as illustrated by one of the earliest microseismic events to be located that occurred around 7 hours after the start of the stimulation (Figure 5a). The second response pattern is illustrated by an event 30 hours after the start of the stimulation (Figure 5b) that has two arrivals, interpreted to be the P and S waves. The minimum traveltimes separation of the P and S arrivals that could be resolved corresponded to hypocentre distances of around 50m. Events for which the P and S arrivals could not be distinguished were even closer to the geophone.

The early events where the P and S arrivals were indistinguishable could be treated effectively as check shots with the shot instant being detected by the deep geophone. Here the onset of the event shown in Figure 5a was taken as time zero of the event and the model granite P and S velocities were simply set at the average velocities from the deep geophone to Otterbach 2. The P and S velocities in the sediments were found by iteratively ray tracing from the deep geophone to the network to find the velocities that gave the minimum RMS traveltimes misfit.

The two-layer model provided reasonable traveltimes fits, with residual errors of up to 23 ms to all the stations except Riehen 2 where the residual P and S misfits were 73 and 97 ms respectively. The Riehen 2 misfits indicate that the velocities are lower to Riehen 2 than to the other receivers. This may be related to faults within a flexure zone that has been mapped near Riehen 2 (Figure 1). However, as the seismicity originates from a relatively small region the ray path differences to the sensors due to different event locations will be correspondingly small. As a result, for location purposes, the residual misfits may be removed by static P and S traveltimes corrections for each receiver station.

### **Microseismic data processing and hypocenter location**

The data acquisition system produced a continuous stream of trace files containing 30 seconds of data. Successive files were read by the data processing software to search for prospective microseismic events. In general a potential event could be reliably identified if the amplitude level at Otterbach 2 exceeded a specified background level as this sensor had very low environmental noise relative to the rest of the network. If there was noise at Otterbach 2 a combination of sensors could be specified to discriminate against noise. This process was continuous and spanned successive data files.

If a potential event was detected the trace data from all of the sensors was extracted for a time window 1s before the trigger and 4s after the trigger and copied to the processing database. An automatic process attempted to pick the P and S times of each new event and perform a location. This process was supported by visual interpretation and typically occupied two interpreters to keep up to date during the stimulation. In this way around 90% of the total event locations were processed in near real time. The remaining events were located subsequently using visual checks to identify missed events and to ensure consistency in the traveltimes interpretation.

The location process was an exhaustive grid search in which an initial coarse location was found using a 25 m cubic grid and a further 2 m cubic grid in the vicinity of the coarse location

to refine the location. For every location, P and S times from Haltingen, Schützenmatte, Riehen 2 and Otterbach 2 were required. The P times from the deep geophone in Basel 1 were also used when this receiver was deployed. For consistency in the locations, any other times were excluded. The hypocenter locations have a maximum rms misfit of 10 ms. Events with larger misfits were not located.

For the located events, moment magnitudes were derived from the principal component of the triaxial sensors required in the location using the spectral method of Abercrombie (1995).

### **Microseismic monitoring and event distribution**

Prior to the main stimulation, 16 locatable microseismic events were detected. The first 4 events coincided with an inflow of water during a drilling operation after the well had reached 4688 m bOD and a further 8 events were located whilst the well was being cemented. Prior to the main stimulation, an injection test was performed in which the pressure was increased very slowly in order to identify the stimulation pressure for seismicity. Initially events occurred sporadically every hour or so. When the surface pressure reached 5MPa the event rate increased to 14 per hour and subsequently continued to increase in line with the rising pressure. However, only 4 events detected during the pre stimulation test were locatable. All of these events prior to the main stimulation occurred close to a permeable zone at 4422m bOD (Figure 8, depth sections 4.2-4.4km and 4.4-4.6km bOD).

The injection rate and wellhead pressure during the main stimulation are shown together with the located microseismic event rate in Figure 6. On 8<sup>th</sup> December an event of 2.6M<sub>L</sub> occurred at 03:06 that had a PGV of 0.55 mm/s and was assigned to the yellow alert level. As a precaution the injection rate was reduced to 1800 l/minute at 04:04 and following further events of >2.0 M<sub>L</sub>, the injection was stopped at 11:34 and the well shut-in. However, a 2.7 M<sub>L</sub> event occurred at 15:46 followed by a 3.4M<sub>L</sub> event at 16:48 on the same day and so in accordance with the response strategy the well was bled off as soon as practicable following the larger event.

A total of 13500 potential events were detected from which 3124 were located in the period 2<sup>nd</sup> to 12<sup>th</sup> December 2006, covering the main stimulation and decline in the event rate. During the post stimulation period from 13<sup>th</sup> December 2006 onwards, a further 350 locatable events were detected up to 2<sup>nd</sup> May 2007 by which time events were occurring sporadically at around one per day. All of the seismicity located during the main stimulation is shown in a 3D view in Figure 7 where the events have been scaled according to their moment magnitudes. More than 80% of the events have misfits of less than 8 ms, the picking error used to estimate the resolution, which suggests that the resolution estimate of 100m is reasonable. The total

volume of the active region has been estimated by summing the volume of a grid of 25 m cubic cells that contain at least 1 event. This produced a volume of just over  $35 \times 10^6 \text{ m}^3$ .

In Figure 8 the event locations during the main and post stimulation are shown for a series of depth slices at 200m intervals where each slice is a contour plot of the number of events in a grid of cells of size 25 by 25 m in the horizontal plane and 200m in depth. The post stimulation events are also shown for the same depth slices as crosses in Figure 8 in order to distinguish them from the main stimulation events.

The depth slices show that the events fall on relatively narrow features. Two distinct orientations can be seen in the microseismicity at N159°E and N120°E (Figure 8, depth section 4.2-4.4km). The post stimulation events to the south of Basel 1, in particular, lie close to a single plane in the dominant orientation, N159°E. This alignment is consistent with the directions of  $S_{Hmax}$  estimated from borehole breakouts at N143±14°E and from drilling induced tensile fractures at N151±13°N and also with the majority of natural fracture orientations in the granite that were in the azimuth range N140°-170°E (Figure 2). In comparison, there were relatively few natural fractures around N120°E which may explain why the microseismic alignments are significantly less developed in that direction. Considering the expected resolution is around 100m, the features in the depth slices could be interpreted as a single fracture surface in the dominant direction with some smaller branches.

## **Migration**

Potential reflections within the microseismic data are of interest as they offer the possibility of imaging fractures that were not seismically active during the stimulation. Such fractures might be targeted by subsequent stimulations or drilling programmes to expand the reservoir. Place et al., 2006 illustrated how steeply dipping faults offset from a geothermal well may be imaged using the VSP method. Here it is shown how potential fractures several kilometres distant from the stimulation well may be imaged by migrating the microseismic trace data.

When the trace data for the located events are displayed for an individual sensor and aligned at either the P or S first arrival picks, near parallel secondary arrivals can be seen (Figure 9). These arrivals are most consistent when the event locations are closest together such as early on in the stimulation (Figure 9, panel A) and so were thought to be potential P and S reflections. In an eight day period around three months after the stimulation, a group of events within ~200m of each other occurred on the southern edge of the reservoir. The traces from these events (Figure 9, panel B) also have consistent secondary arrivals but at different times to those in Figure 9, panel A that are due to source locations ~800m away.

In order to image the potential reflectors a 3D diffraction stack type migration (e.g. Chavarría et al., 2003) was applied to the events located during the stimulation and post stimulation up to 2<sup>nd</sup> May 2007. P wave images were formed separately by applying a tapered mute prior to the direct S wave arrival. The signal to noise ratio of the P wave was strongest on the vertical traces as would be expected and so the P wave migration images were formed using the vertical traces only. The S wave arrival was strongest on one or other of the horizontal traces. The horizontal trace with the best signal to noise ratio was used to form the S wave migration images. In this case a mute was applied to eliminate the direct P and S waves.

Each sensor was migrated separately as the sensors were too widely spaced to produce continuity in a stacked image of more than one sensor. Initially no constraints were applied to the dip and azimuth of the reflectors in the images. For example, horizontal and vertical sections through the Schützenmatte S wave migration are shown in Figure 10. Two assumed faults from Figure 1 have been overlaid on the Schützenmatte migration for reference. Whilst it is interesting to note the coincidence of migration features and the fault traces in the horizontal section, the migration data are not sufficiently reliable to be correlated with the assumed faults to make an interpretation.

Steeply dipping features aligned around N150°E appeared to be preferentially enhanced in all the images to the north east of Basel 1. The images to the west of Basel 1 showed no preferential directions of stack response and so are not considered here. In order to optimise the observed alignments, secondary migrations of the region east of Basel 1 were performed with an aperture control applied to constrain the azimuth of the reflectors to N150±5°E. The dip was constrained to 87±5° in the direction N240°E to be in keeping with the overall dip of the microseismicity. Beyond this range the trace amplitudes included in the stack were tapered linearly to zero over a further 5°.

For illustration, sections through the Schützenmatte P and S wave migration images with aperture controls are displayed in Figure 11 for horizontal and vertical sections with the maximum amplitude. The P wave images cover a smaller region than the S waves due to the limited trace range between the direct P and S wave arrivals that could be migrated as potential P wave reflections. Also, the P wave image has lower resolution due to the longer P wavelengths. The P and S wave images have been shown for the same region in Figure 11 for ease of comparison.

There is a reasonable degree of consistency between the P and S wave images in Figure 11. All the images suggest there may be three reflectors to the east of the event locations that are indicated by black lines shown in the same position overlying the P and S wave images. The strike of these features is around 145°, which is consistent with the overall strike direction of the microseismicity. The apparent dips are less than the overall dip of the microseismicity and

are around or less than the shallow dip extent of the allowed dip range. This may be due to migration smearing rather than the real dip.

The features are offset 600, 1050 and 1600m from Basel 1 and so would be of interest for targeting further boreholes to develop a more extensive reservoir in this region. However, these potential reflectors are not imaged unambiguously. The limited distribution of events and migration of a single sensor means that the migration process cannot stack out noise effectively and it is assumed there is a possibility that the images are migrated noise. To obtain more reliable images a larger number of receivers would be required either by expanding the network considerably or by deploying a multi-level string in one or more boreholes.

## **Discussion**

The estimated, stimulated volume containing seismically active fractures is of the order of 10% of the target volume of  $400 \times 10^6 \text{ m}^3$ . Due to the occurrence of the larger seismic events it is not yet clear whether further work to enhance the fractured volume can be performed in the future. Whilst the intention was to produce microseismicity associated with fracture opening to improve the injectivity of the reservoir, the events were larger than anticipated based on previous experience at other HDR sites. This problem is the subject of continuing research efforts to understand the mechanisms of larger events and identify potential means of avoiding such events during stimulation and production.

None the less, the subject of this paper, the microseismic monitoring system, was reliable and was considered to be a technical success. In cooperation with the SED, earthquake magnitudes were derived in near real time and were published on the web for public information. Although the larger earthquakes were undesirable, the response strategy provided an effective means of dealing with these events in a consistent manner and was essential in fulfilling the exploration company's overriding commitment to public safety. The microseismic system also provided important technical information for monitoring and evaluating the hydraulic stimulation as the event locations and time history enabled the growth of the stimulated region and its dimensions to be assessed in near real time.

It appears that the stimulation has produced a relatively thin fractured region or possibly a single fracture surface with a few smaller branches providing additional lateral extent. The overall reservoir strike direction is consistent with the azimuth of  $S_{Hmax}$  and the strike direction of natural fractures within the crystalline section from UBI log analysis. Imaging of the fine structure of the reservoir has been possible due to the relatively good resolution of the event locations. This was due to a combination of careful traveltimes interpretation, consistent

location criterion and a reliable velocity model.

Obtaining the velocity model from geothermal wells can be difficult using check shots due to the high temperatures and pressure conditions downhole that the explosives must be able to operate under reliably and safely. It has been reported that one alternative method using drilling jars had only limited success. A second, novel method using a special high temperature and pressure geophone tool in the injection well succeeded and was relatively economic and involved much less risk to the well in comparison to firing check shots. This new technique is likely to be useful in other geothermal applications and possibly elsewhere.

It has also been shown how 3D migration can take the exploration a step further by enabling potential fracture zones that have not been stimulated to be imaged. If this technique can be developed into a reliable method, it could be significant in planning the trajectories of subsequent wells to optimise energy production and in assessing the economic potential and reservoir development costs.

### **Acknowledgements**

We thank the investor group Geopower Basel AG for their continuing financial commitment and support. The authors gratefully acknowledge the continuing contribution of the Swiss Seismological Service. Expert advice in ground velocity measurements was kindly provided by Adrian Egger of Rutishauser Ingenieurbüro GmbH. The hydraulic data were diligently acquired by GEO-data and we are indebted to Claudio Forlin for his prompt IT support. We would also like to acknowledge the contributions of the following specialist suppliers of equipment for the permanent microseismic system. The data acquisition system was supplied by Reftek. Network sensors were supplied by SonDI and Consultants. Microseismic processing software and high temperature and pressure seismic tools used in Basel 1 were supplied by Semore Seismic Ltd.

### **References**

Abercrombie, R. E. (1995). Earthquake source scaling relationships from -1 to 5 ML using seismograms recorded at 2.5 km depth, *Journal of Geophysical Research*, 100, 24,015-24,036.

Baria, R., Jung R., Tischner, T., Nicholls, J.D.N., Michelet, S., Sanjuan, B., Soma, N., Asanuma, H., Dyer, B. and Garnish, J., 2006. Creation of an HDR reservoir at 5000m depth at the European HDR project. Proceedings of the 31<sup>st</sup> Workshop on Geothermal Reservoir Engineering, Stanford University, California. January 30-February 1, 2006. SGP-TR-179

Baria R., Michelet S., Baumgaertner J., Dyer B., Gerard A., Nicholls J., Hettkamp T., Teza D., Soma N., Asanuma H., Garnish J. Microseismic monitoring of the world's largest potential HDR reservoir. Proceedings of the 29th Workshop on Geothermal Reservoir Engineering, Stanford University, California. January 26-28, 2004.

Chavarria, J.A., Malin, P., Catchings, R.D. and Shalev, E., 2003. A Look Inside the San Andreas fault at Parkfield Through Vertical Seismic Profiling. *Science*, 5, 1746–1748, DOI: 10.1126/science.1090711.

Evans, K., and P. Roth (1998), The state of stress in northern Switzerland inferred from earthquake seismological data and in-situ stress measurements, final report, Deep Heat Mining. DHM, Steinmaur, Switzerland.

Gürler, B., Hauber, L. and Schwander, M., 1987. Die Geologie der Umgebung von Basel mit Hinweisen über die Nutzungsmöglichkeiten der Erdwärme, Schweizerische Geologische Kommission, Bern.

Illies, J.H., 1981. Mechanism of Graben formation. *Tectonophysics*, 73(1-3): 249-266.

Julian J. Bommer, Stephen Oates, José Mauricio Cepeda, Conrad Lindholm, Juliet Bird, Rodolfo Torres, Griselda Marroquín and José Rivas, 2006. Control of hazard due to seismicity induced by a hot fractured rock geothermal project. *Engineering Geology* 83 (2006) pp 287-306.

Lacombe, O., Angelier, J., Byrne, D. and Dupin, J., 1993. Eocene-Oligocene tectonics and kinematics of the Rhine-Saone continental transform zone (Eastern France). *Tectonics*, 12(4): 874-888.

Laubscher, 1970. Grundsätzliches zur Tektonik des Rheingrabens. In: J.H. Illies and S. Mueller (Editors), Graben Problems. Proceedings of an International Rift Symposium held in Karlsruhe 1968, 79-86.

Place J., Naville C., Gerard A. and Schaming M., 2006. Oriented three components VSP method applied to imaging highly dipping faults in the deep granite basement at Soultz-sous-fôrets. ENGINE workshop, Potsdam, 2006.

Plenefisch, T., Bonjer, K.-P. (1997). The stress field in the Rhine Graben area inferred from earthquake focal mechanisms and estimation of frictional parameters, *Tectonophysics* 275,

pp. 71-97.

Rutishauser Ingenieurbüro für Bau, Verkehr und Umwelt GmbH, Zürich (2006). Erschütterungstechnische Beratung. Report to Geopower Basel AG for Swiss Deep Heat Mining Project, Basel, 5121/01/AE/RU.

Tester J.W., Anderson B.J., Batchelor A.S., Blackwell D.D., DiPippo R., Drake E.M., Garnish J., Livesay W., Moore M.C., Nichols K., Petty S., Toksöz N.M. and Veatch R.W., 2006. The Future of Geothermal Energy. Massachusetts Institute of Technology report INL/EXT-06011746. ISBN:0-615-13438-6.

Ustaszewski, K., Schumacher, M.E., Schmid, S.M. and Nieuwland, D., 2005. Fault reactivation in brittle-viscous wrench systems - dynamically scaled analogue models and application to the Rhine-Bresse Transfer Zone. *Quaternary Science Reviews* 24, 363-380, doi:10.1016/j.quascirev.2004.1003.1015

Valley, B., Evans, K.-F. (2006). Stress orientation at the Basel geothermal site from wellbore failure analysis in Basel 1, ETH Report Nr.: ETH 3465/56.

## Figures

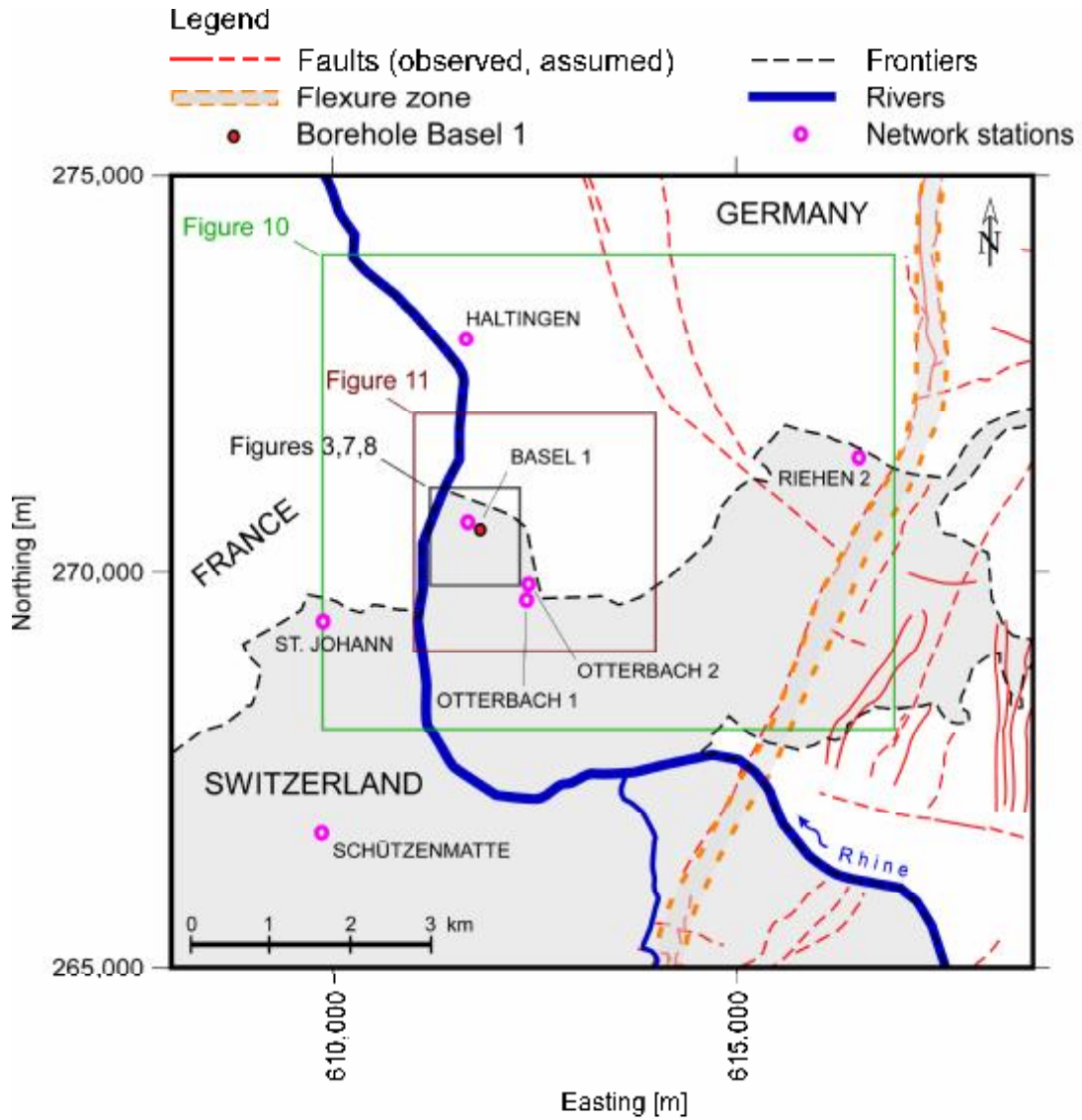
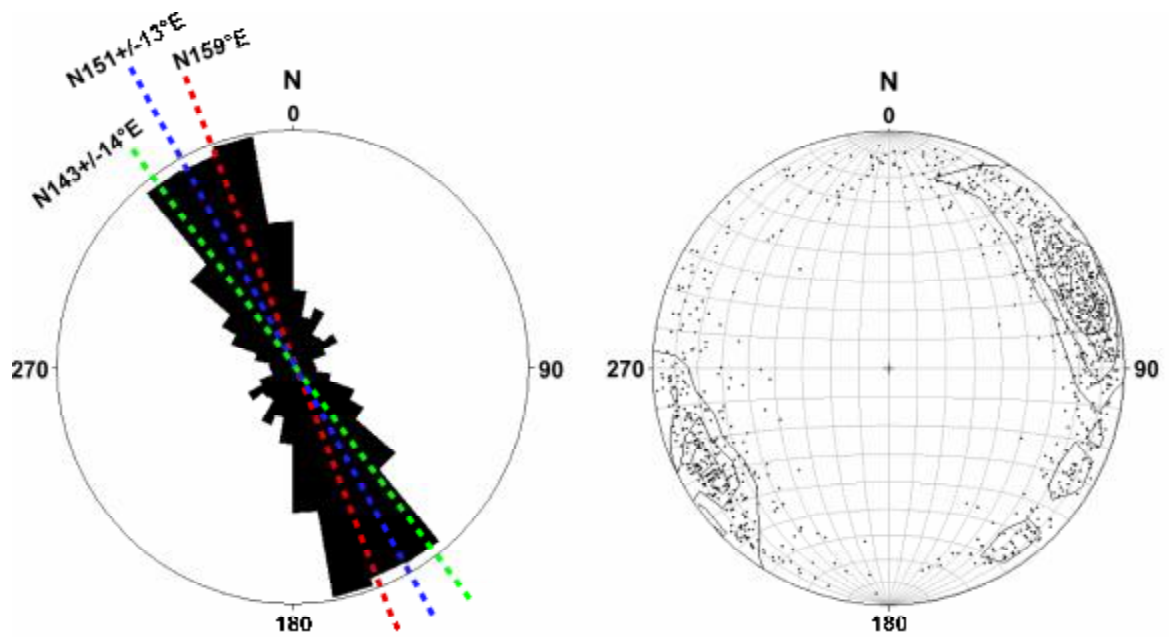


Figure 1. Tectonic map of the Upper Rhine Graben. The location of the borehole Basel 1 and the microseismic monitoring network stations are shown as red dots. The frames indicate the boundaries used in subsequent figures. After Gürler et al. (1987).



Rose diagram

Stereoplot

- strike direction of natural fractures and joints
- azimuth of  $S_{Hmax}$  for borehole breakouts
- azimuth of  $S_{Hmax}$  for drilling induced tensile fractures
- Reservoir strike direction

Figure 2. Orientation of natural fracture planes and joints. Strike direction, left, and orientation of the fracture and joint plane normals in a stereoplot, right. Superimposed on the left diagram are the mean directions of  $S_{Hmax}$  from borehole data and the reservoir strike direction from the microseismic data.

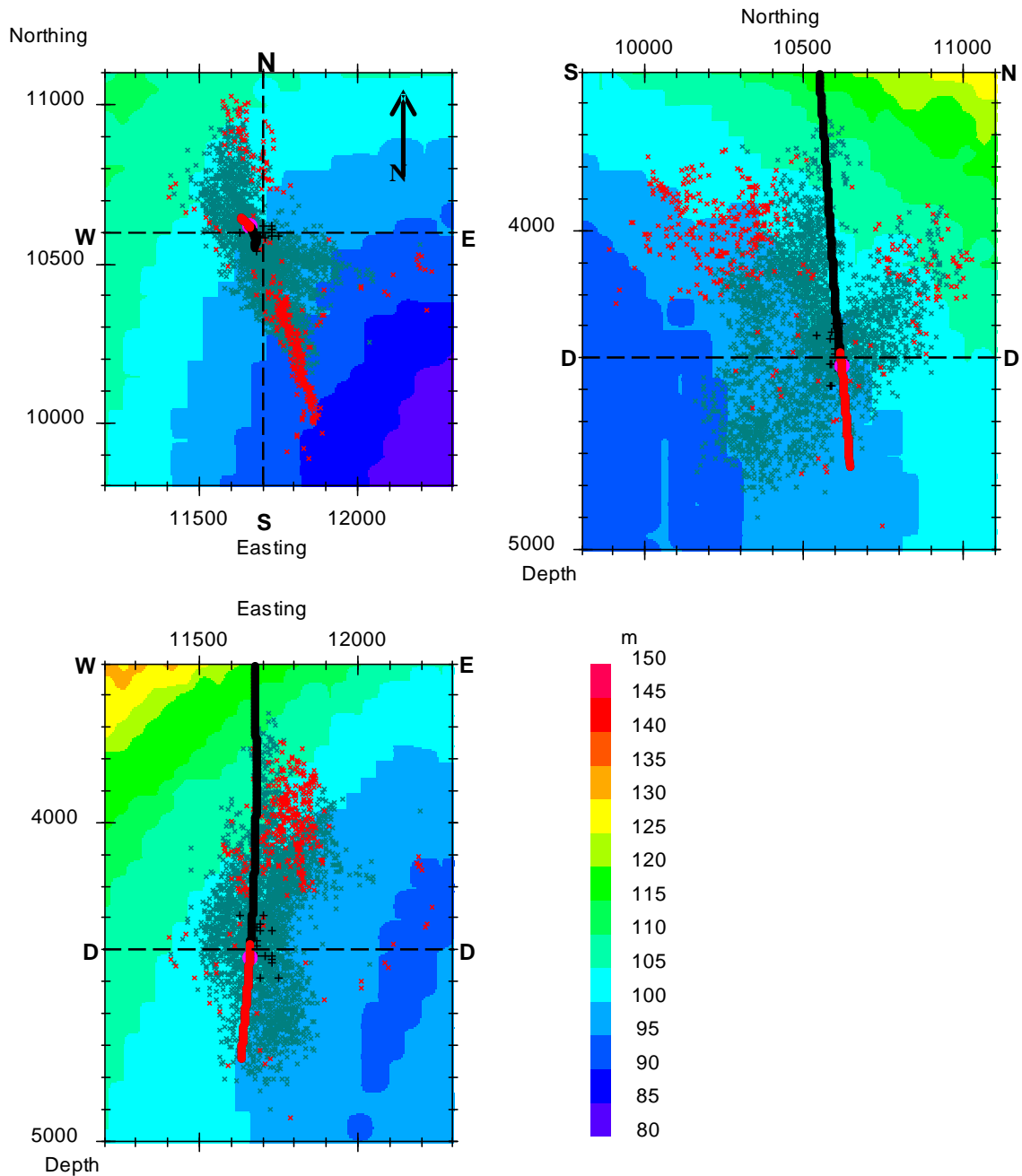


Figure 3. Model network resolution for a constant velocity model,  $V_p=5.94\text{km/s}$  and  $V_s=3.45\text{km/s}$ , and picking accuracies of  $T_p=\pm 8\text{ ms}$  and  $T_s=\pm 8\text{ ms}$ . Clockwise from top left are an horizontal section (DD) at 4400m depth, South to North (SN) section at 11700m East and West to East (WE) section at 10600m North. The local coordinates shown are the map (Figure 1) Easting-600,000m and the map Northing-260,000m. The intersection of the vertical sections with the horizontal section are indicated by the dotted lines marked SN and WE and the intersection of the horizontal section with the vertical sections is indicated by the dotted lines marked DD. The cased section of the Basel 1 borehole is indicated by the solid black line and the openhole portion is shown in red. The pre stimulation, main stimulation and post stimulation events are shown as black, green and red crosses respectively.

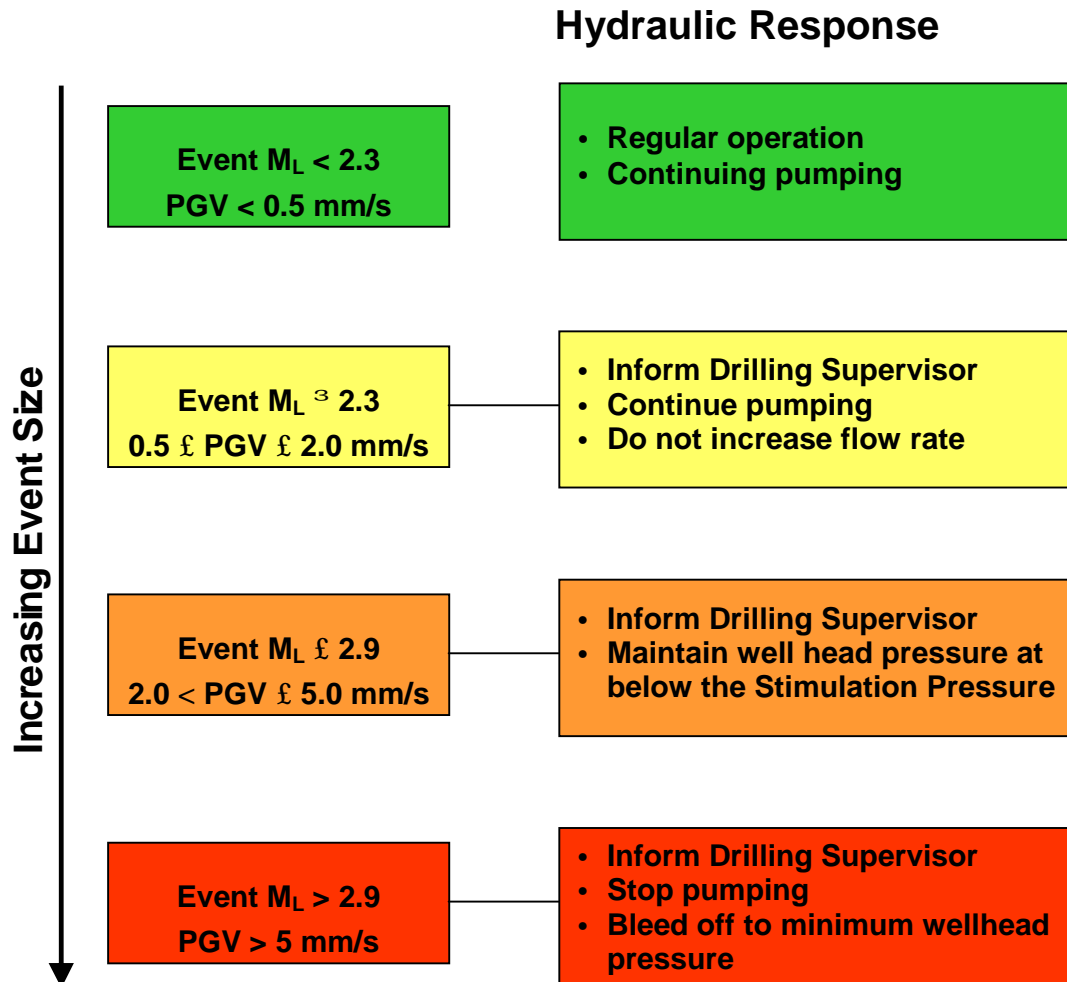


Figure 4. Seismic response procedure.  $M_L$ , Local Magnitude and PGV, Peak Ground Velocity, both provided by the Swiss Seismological Service.

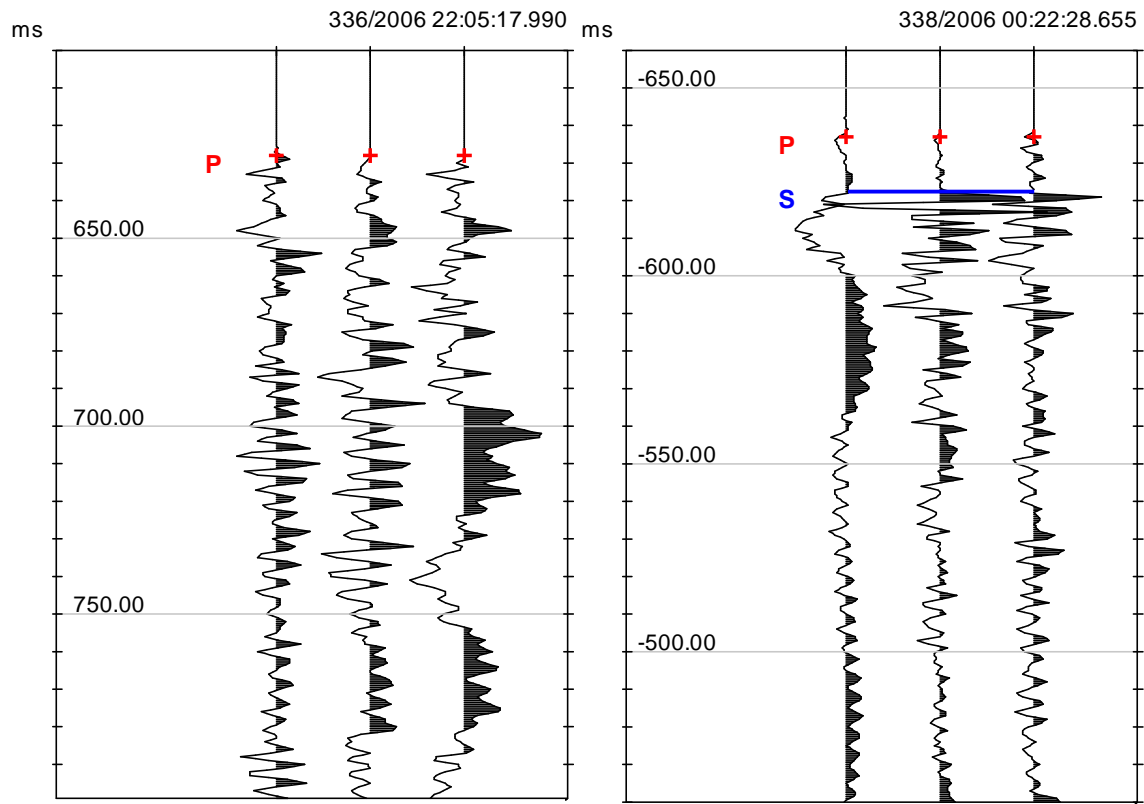


Figure 5. Two events recorded by the geophone in BS1. The traces are displayed in the order vertical, horizontal 1 and horizontal 2. The group on the left are from the first event to be located and do not have a distinct S wave arrival. The group on the right were recorded around 26 hours later and have distinct P and S arrivals. The P to S time difference corresponds to an event offset from the sensor of around 115m.

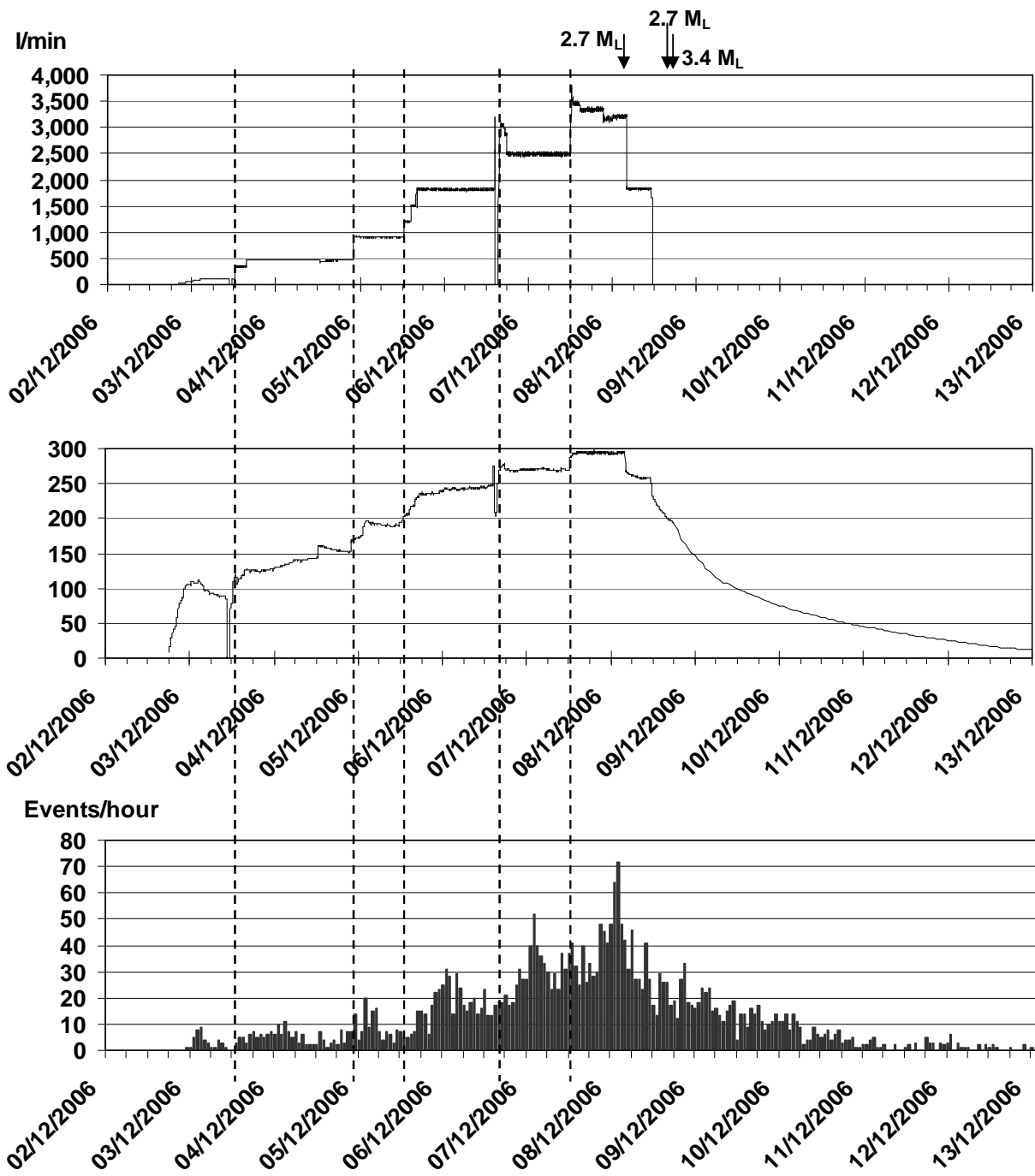


Figure 6. Basel 1 main stimulation hydraulic and seismic data. From top to bottom, the injection rate, surface injection pressure and the located seismic event rate. The anomalous hydraulic values on 3/12 and 6/12 relate to periods in which the injection pumps were being exchanged. The three largest events are indicated for reference to the hydraulic data.

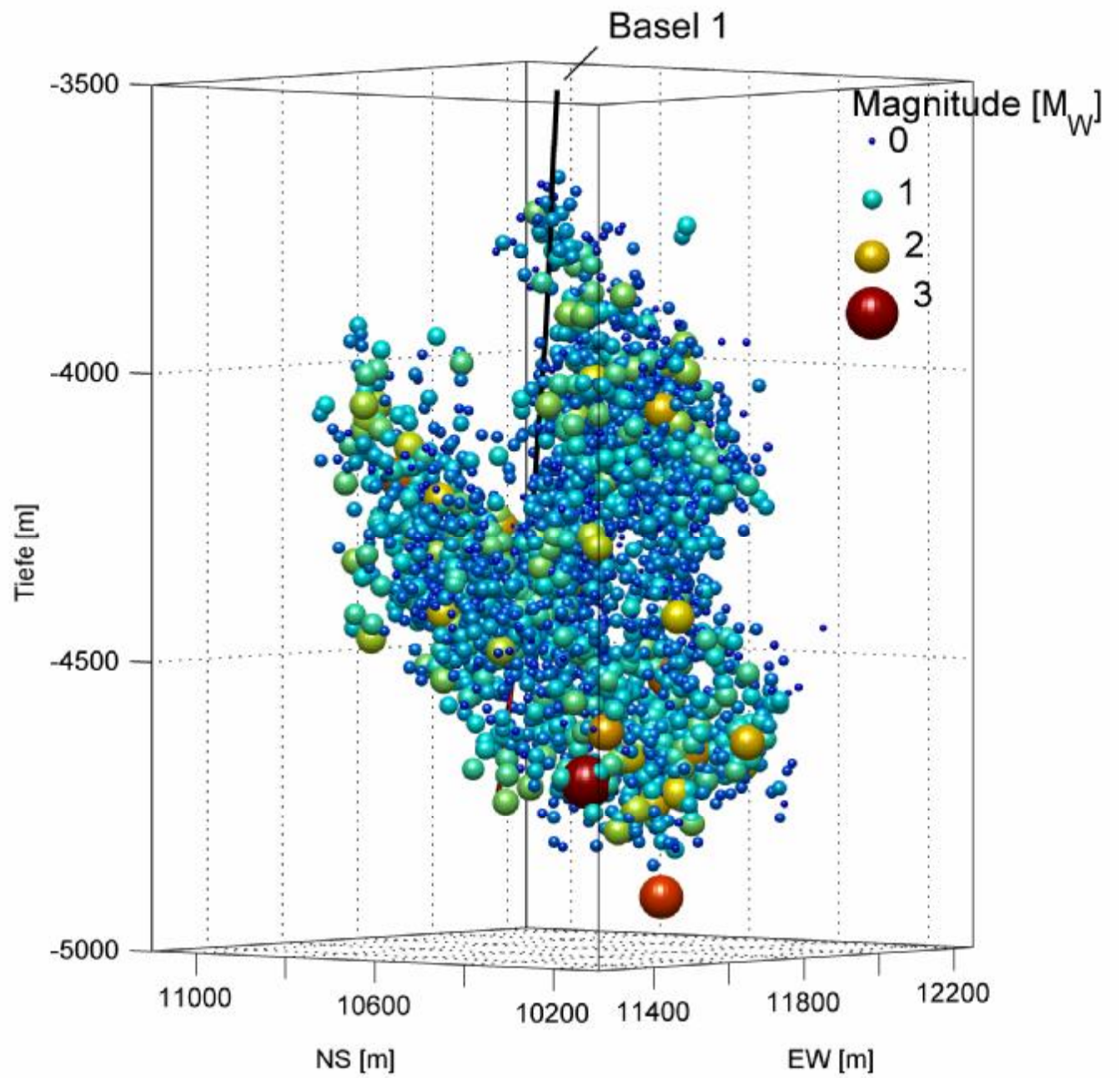


Figure 7. 3D view of the microseismic events detected during the main stimulation with the event symbols coloured and scaled according to the Moment Magnitudes.

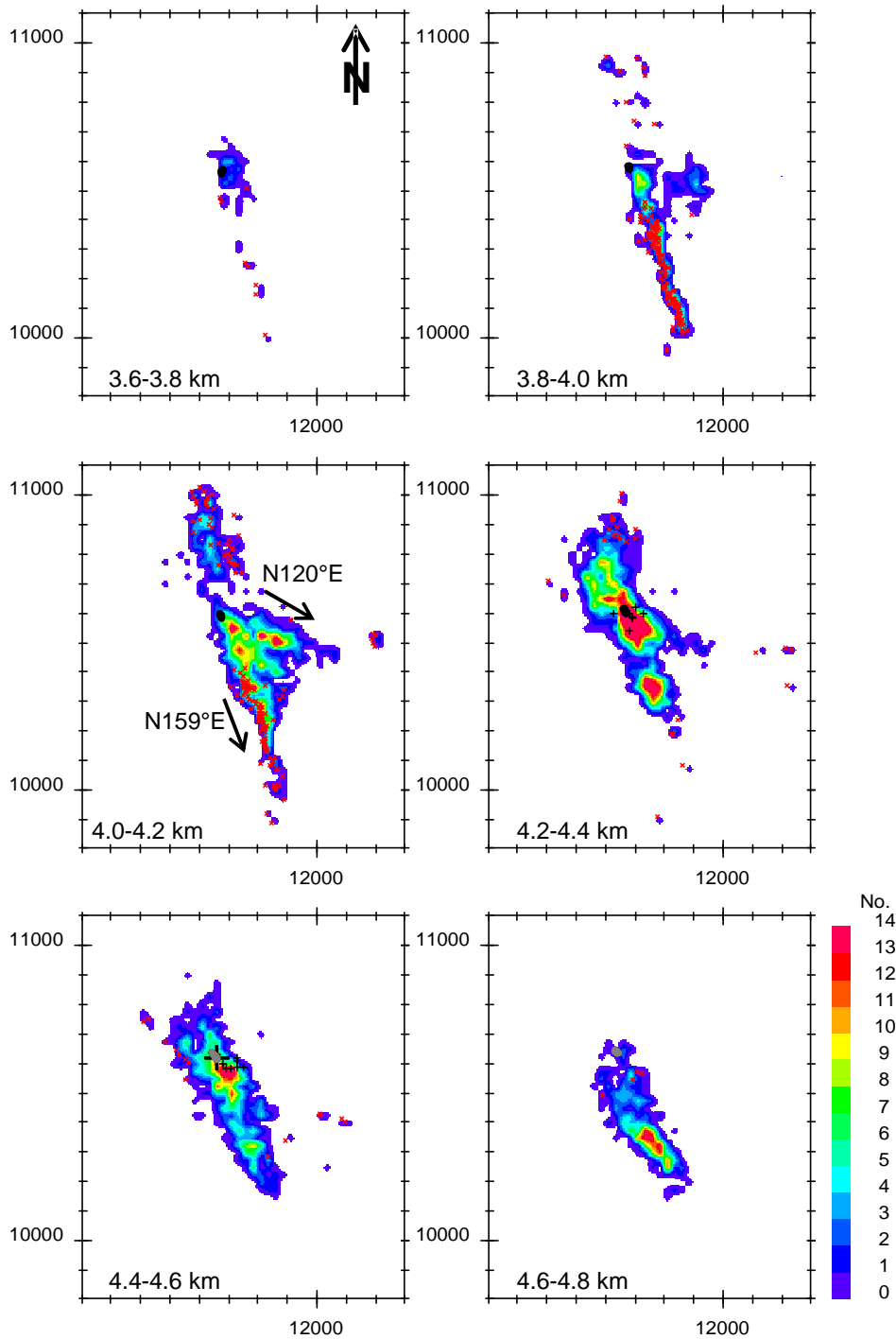


Figure 8. Depth slices between 3.6 and 4.8 km bOD showing contours of the number of seismic events during the main and post stimulation phases in a grid of cells 25x25x200m. The depth range bOD of each slice is annotated in the bottom left hand corner. The pre and post stimulation events are overlain as black and red crosses respectively. The projection of the BS1 borehole in each depth section is shown in black for the cased section and grey for the openhole. The large black cross in the 4.4-4.6 km section indicates the location of the Basel 1 geophone.

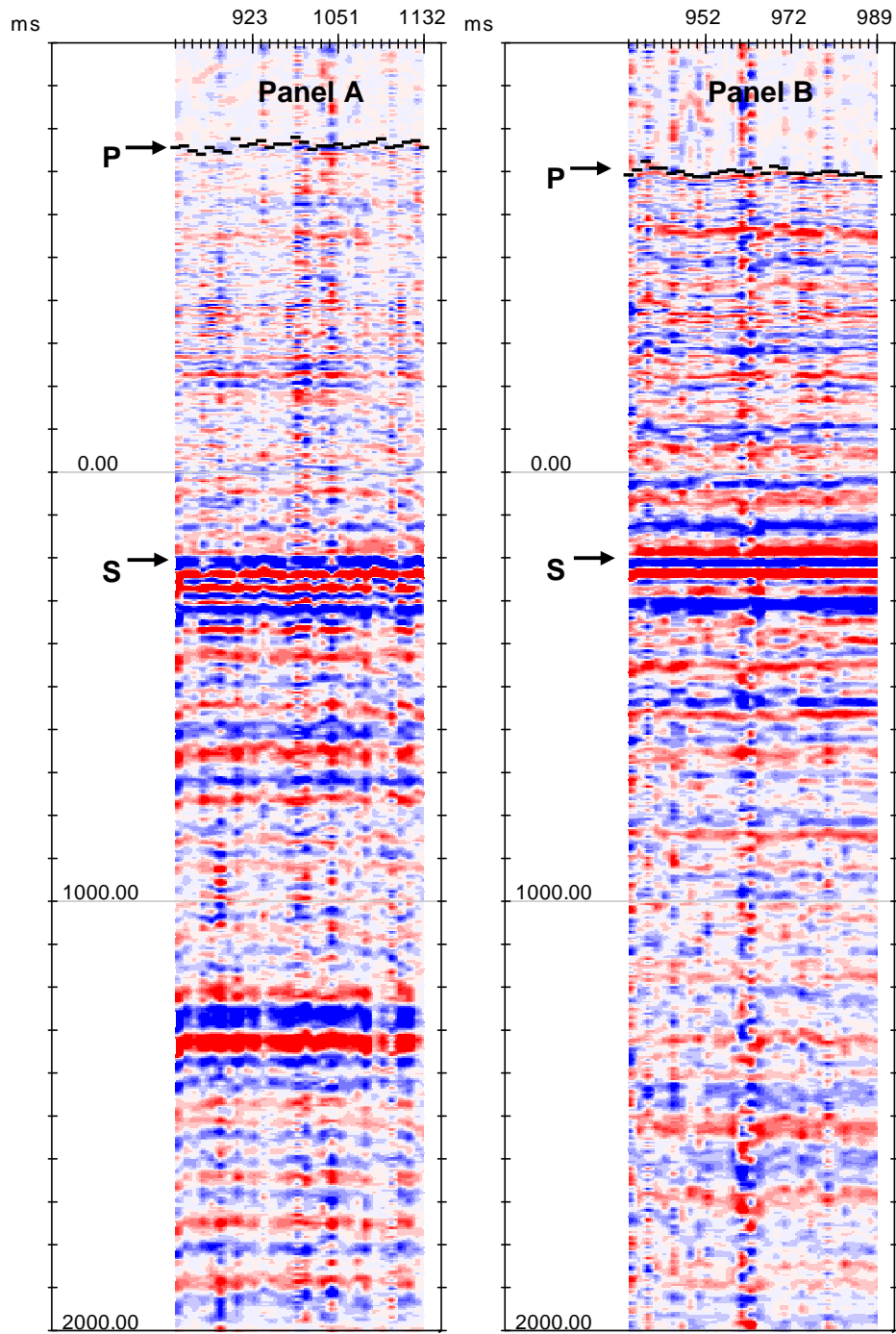


Figure 9. Common receiver gathers of the vertical trace at Schutzenmatte. Panel A covers a 12 hour period at the start of the stimulation. Panel B covers an 8 day period 3 months after the stimulation. The traces have been aligned with the direct S wave at 200ms. The P wave picks are indicated by horizontal black bars. DC removed, trace by trace scaling, 300% overlap.

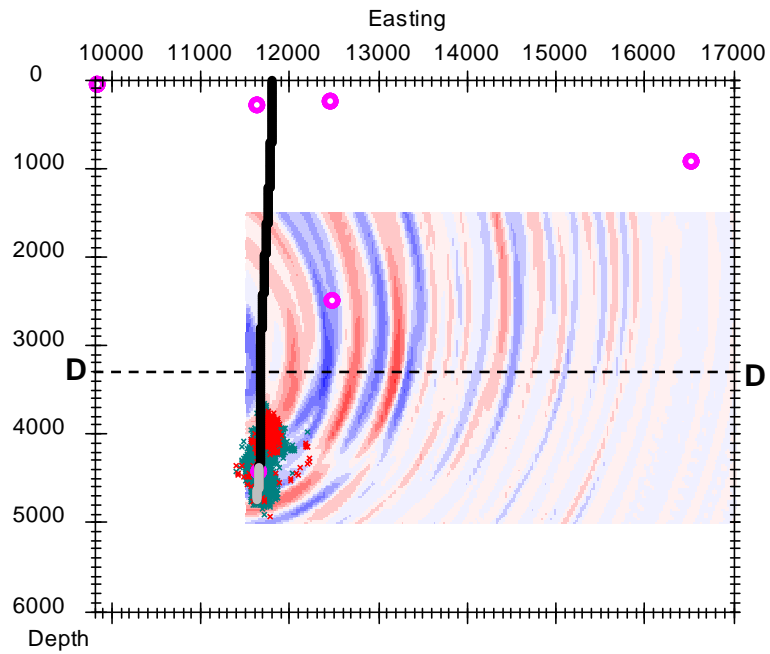
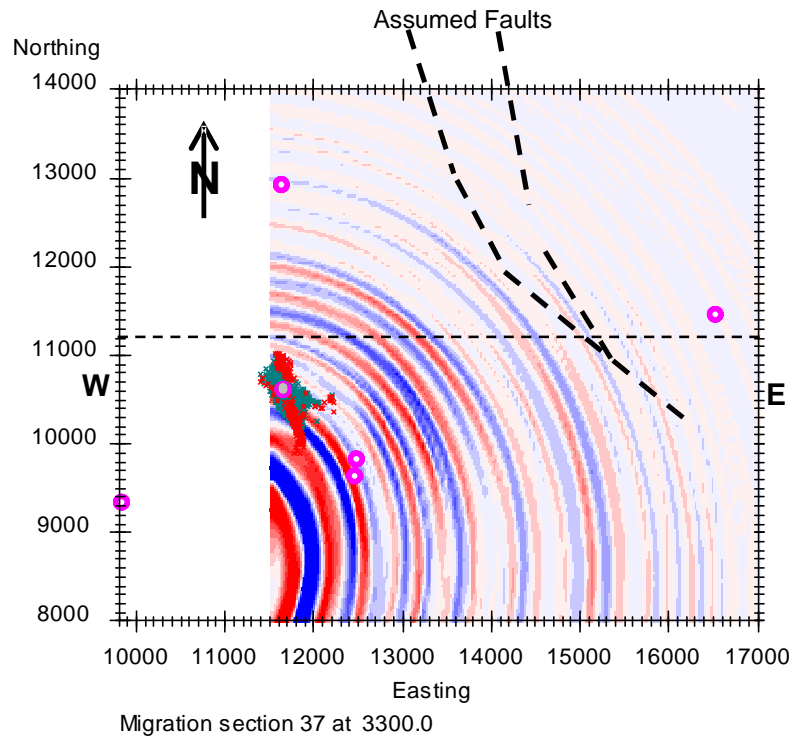


Figure 10. S wave migration at Schützenmatte in an horizontal section, top, at 3300m depth and a vertical W-E section, bottom, at 11200m North. The intersection of the vertical section with the horizontal section is indicated by the WE dotted line and the intersection of the horizontal section with the vertical section is indicated by the dotted line DD. The assumed faults previously shown in Figure 1 are overlain in the horizontal section for reference and the coordinates are related to the map as given in Figure 3. The main stimulation and post stimulation events are shown as green and red crosses respectively. The cased section of Basel 1 is shown in black and the openhole is shown in grey. The pink circles mark the microseismic monitoring network stations. Schützenmatte is west of the figure boundary.

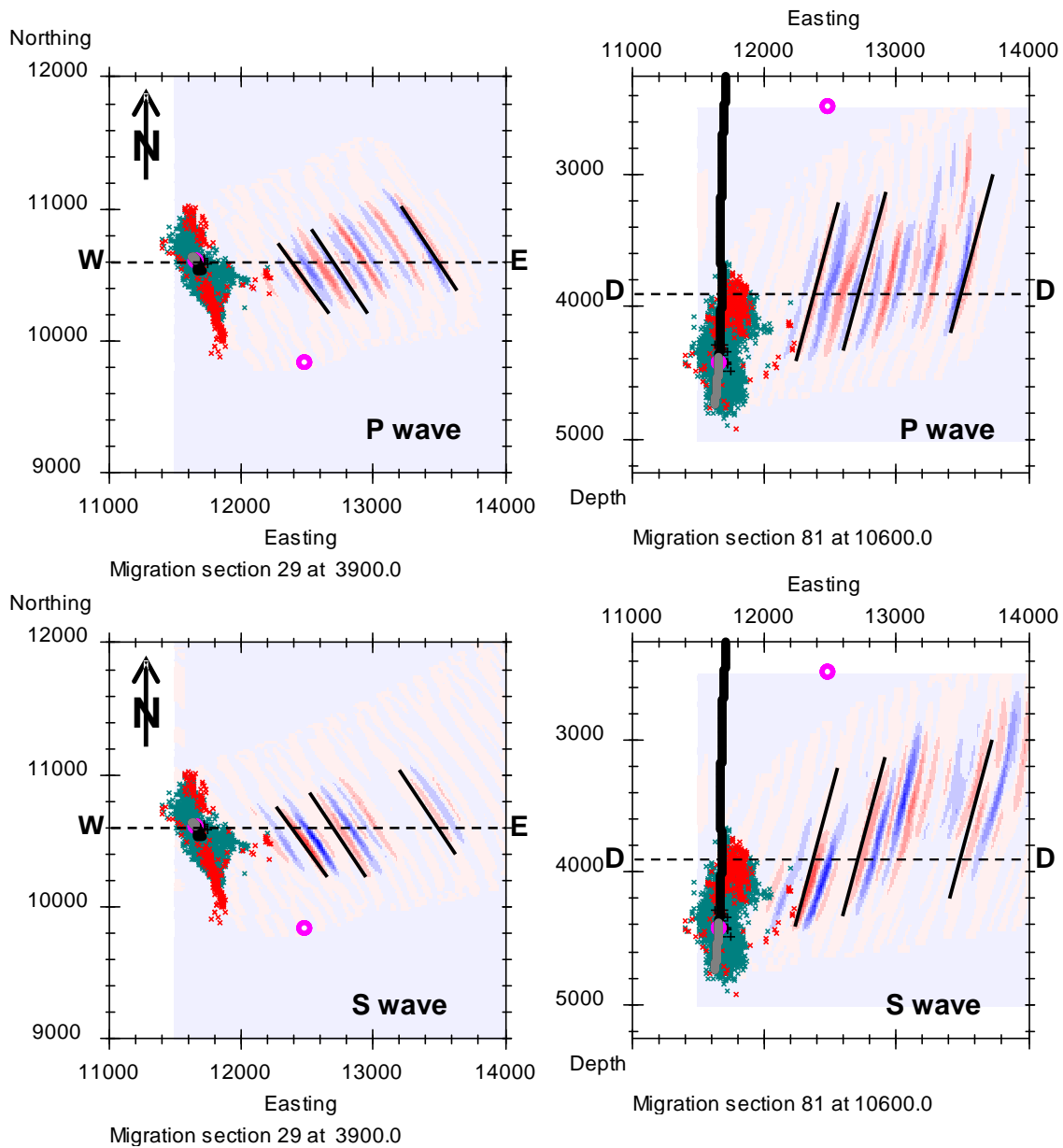


Figure 11. The P wave and S wave migrations with aperture control at Schützenmatte in horizontal sections at 3900m depth, left hand side, and vertical W-E sections at 10600m North, right hand side. The intersection of the vertical sections with the horizontal sections are indicated by the WE dotted lines and the intersection of the horizontal sections with the vertical sections are indicated by the dotted lines DD. The black lines indicate the strike and dip of the three interpreted reflections. The pre stimulation, main stimulation and post stimulation events are shown as black, green and red crosses respectively. A 500m, low pass filter has been applied from left to right across the sections. The cased section of Basel 1 is shown in black and the openhole is shown in grey. The pink circle is the Otterbach 2 station.